International Journal of Thermal Sciences 184 (2023) 107882

Contents lists available at ScienceDirect

International Journal of Thermal Sciences

journal homepage: www.elsevier.com/locate/ijts

Heat transfer characteristics of mildly rarefied gaseous flows in the slip regime

Ambuj Amitab Jha, Amit Agrawal *

Department of Mechanical Engineering, Indian Institute of Technology Bombay, Mumbai, 400076, India

ARTICLE INFO

Keywords:
Knudsen number
Nusselt number
Brinkman number
Pressure work
Viscous dissipation

ABSTRACT

The present numerical work aims to delineate the heat transfer characteristics present in mildly rarefied gaseous Nitrogen flows with comparable Knudsen number throughout the flow domain. The principal objective is to analyze the behavior of the resulting thermal flow field with an increasing degree of rarefaction and to establish the dependence of Nusselt number on Knudsen number and Reynolds number. The current analysis deals with the flow through an isothermally heated circular pipe with a temperature of 350 K at the heating wall. The ranges of mean Knudsen numbers and Reynolds numbers considered in the analysis are $(0.0009 - 0.09)$ and $(20 - 0.004)$, respectively. These correspond to a pressure ratio less than 1.03 in all the test cases. The coupled set of governing equations are solved using the finite volume method algorithm SIMPLEC in FLUENT 2020-R2. The results are validated with the experimental results from Hemadri et al. [1] to authenticate the adopted solution methodology. Notably, with increasing Knudsen number, the fully developed Nusselt number is found to attain a maximum value of about 4.022 corresponding to Knudsen number ≈ 0.006 and Reynolds number ≈ 0.468. The fully developed Nusselt number starts dropping monotonically with a further rise in Knudsen number. The axial span of the thermally fully developed region is also observed to follow this pattern qualitatively with rising degree of rarefaction. Importantly, Brinkman number is seen to increase from about0 to 1 for each test case. All the same, the strength of viscous dissipation remains negligible in the complete flow domain. The rate of increase in the kinetic energy due to expansion work is observed to become marginally small with increasing rarefaction. These findings confirm that the rate of pressure work, viscous stress work at the wall, and viscous dissipation need not be considered for such practical situations. The defining factors that govern the overall heat transfer phenomena are advection, conduction, and the amount of non-equilibrium of the fluid parcels near the wall. These findings also defend the argument that the heat transfer correlations cannot be generalized in terms of Brinkman number or Peclet number only. Instead, they need to be formulated separately depending on the operating conditions of the problem.

1. Introduction

The emerging needs for energy-efficient and miniaturized devices have stimulated numerous studies in the field of rarefied gaseous flows. The need for optimally designing passages for the heat exchangers presents itself frequently. To accomplish so, the first requirement is to understand the underlying physics behind the associated flow phenomena and the respective quantities of interest. Works have been exercised in profusion in the last three decades towards this and useful literature reviews can be referred from Agrawal et al. [2] and Kandlikar et al. [3]. The similarity parameter that classifies such flows is Knudsen number (Kn). It is defined as the ratio of the mean free path between two successive collisions of molecules (λ) and the passage dimensions; $Kn = \lambda/D$ for pipe flows with inner diameter D. It has unanimously been recognized that as Kn starts increasing beyond 10^{-3}, the gas molecules near the pipe wall no longer maintain equilibrium with the wall, thus resulting in tangential velocity slip and temperature jump at the wall. Study of mildly rarefied gaseous flows in the slip regime is discussed in the present work. While undergoing heat transfer, such flows may simultaneously exhibit different effects such as non-equilibrium at the wall, axial conduction, expansion work and viscous stress work. Several approachable methods have been reported in the literature to highlight the flow behavior resulting from these effects. However, due to the assumptions predisposed towards obtaining the solution, the results are

* Corresponding author.
E-mail address: aagrawal.iitb@gmail.com (A. Agrawal).

https://doi.org/10.1016/j.ijthermalsci.2022.107882
Received 26 June 2022; Received in revised form 14 August 2022; Accepted 18 August 2022
Available online 13 September 2022

neither found to be in harmony among themselves, nor with the physical reality. To start with, we briefly discuss some of the studies done progressively in this field. The needs to probe deeper into this field are then pointed out, followed by the objectives of the present work.

One among the first studies on the heat transfer aspects of slip-flows in the fully developed region was carried out analytically by Sparrow and Lin [4]. Axial advection and radial conduction terms were retained in the energy equation, with the rest terms dropped. This corresponds to the well-known classical 'Graetz problem'. It was reported that the fully developed Nusselt number (Nu_{fd}), which represents the axially non-varying non-dimensionalized heat transfer coefficient, is lower than the continuum cases and it continues to decrease with increasing *Kn*. The analytical work done by Ou and Cheng [5] on the flow of ideal gases in the continuum regime considered the addition of pressure work and viscous dissipation terms to the Graetz problem. They reported that the pressure work and viscous dissipation effects balance each other to render a constant bulk mean temperature. The analysis was extended by Hadjiconstantinou [6] for small scale gaseous flows including the viscous stress work at the wall that was first highlighted briefly by Maslen [7] and later by Hong and Asako [8]. Nu_{fd} was found to drop continuously over the small range of Brinkman number (Br) considered, where *Br* represents the ratio of rate of viscous heat dissipation to the rate of heat exchange between the wall and the fluid. These studies did not consider axial conduction and property variation, thus further limiting the ranges of *Kn* or *Br* over which the solution can be utilized. The axial conduction and viscous dissipation effects were included in the works by Jeong and Jeong [9] and Cetin et al. [10] while the pressure work term was ignored. A detailed numerical examination was done by Sun and Jaluria [11] where all the terms in the energy equation along with the property variation were retained. Large inlet to outlet pressure ratios were specified in their trials. Local *Nu* was found to increase along the downstream after passing a small span of the thermally fully developed region. The influence of viscous stress work at the wall was not taken into account. The exact solutions of Falkner-Skan flow over a specific wedge-shaped surface and through a converging channel was obtained in the analysis done by Turkyilmazoglu [12,13]. The conventional analysis was extended in this work to include velocity slip and temperature jump at the boundaries. Haddout and Lahjomri [14] analyzed the extended Graetz problem involving pressure work and viscous dissipation using the self-adjoint formalism. They used slip flow Poiseuille velocity profile with constant properties. Similar set of assumptions were considered in the numerical work done by Ramadan [15] for gas flow in a microtube with constant heat flux. To quantify the extent of heating near the wall due to finite viscous stress work, surface energy balance between the wall and the fluid is utilized. This leads to two definitions of *Nu*: a) diffusive *Nu* that only accounts for the diffusion of heat from wall to the fluid without considering the viscous heating at the wall, and b) total *Nu* which considers the viscous stress work at the wall as well. In the recent study done by Nicolas et al. [16], complete set of governing equations with constant properties were numerically solved. For mildly rarefied slip flows, it was reported that the net heat transfer from the wall in the fully developed region is negligible. The constant diffusive *Nu* was found to be entirely due to the viscous stress work at the wall. Further, for compressible slip flows the fully developed total *Nu* was found to drop continuously with rise in *Kn*. Perturbation method was used to obtain the closed form solutions involving effects of rarefaction, compressibility, inertia and viscous dissipation by Guranov et al. [17]. However, viscous stress work at the wall was ignored and the solutions were reported only for the fields of pressure, velocity and temperature.

A few crucial sides that emerge from the available literature requiring detailed examination include: (i) The studies emphasize different combinations of effects to approach the solution. However, consideration of these effects depends on the flow conditions such as pressure ratio and supplied wall temperature, among others; (ii) A majority of the referred works have imposed a uniform temperature entry condition at the inlet to the heating region. This does not hold for physical situations where the backward axial conduction is significant; (iii) Most of the works do not consider the variation of thermophysical properties while applying large pressure ratios; (iv) The trends for the variation of *Nu* along the flow from different studies are not found in agreement. This is an inherent implication of the assumptions taken to obtain the solution.

Since the presence of different effects depends on the flow conditions, present study focuses on mildly rarefied slip flows that involve comparable *Kn* throughout the flow domain. This ensures the validity of our reported variation of local and fully developed *Nu* with *Kn* and *Re* (Reynolds number). *Re* indicates the strength of inertial forces in comparison with viscous forces; $Re = \rho \bar{v}_z D/\mu$. Here ρ is fluid density, $\bar{v}_z$ represents mean axial velocity and μ is viscosity. Such heat transfer applications are often encountered where the pressure drop along the flow is relatively small. Optimal calculations are desired with regard to the size of the required system of heat exchangers. To meet these needs, the present study aims to address: (i) the relative dominance of the effects of each term in the energy equation in defining the flow field, (ii) the effect of viscous stress work at the wall to decide for its inclusion in the thermal analysis in practical scenarios, (iii) the reliability of the reported *Nu* trends with *Br* or *Kn*, and (iv) the serious pitfalls that the imposed assumptions may implicate. These objectives are achieved by solving the complete set of governing equations for mass, momentum and total energy. The case of isothermally heating wall at 350 K is selected for the analysis with mean *Kn* and *Re* ranging from (0.0009 to 0.09) and ($20 - 0.004$), respectively. The property variation is retained to examine their effect. The effects of all the factors in the energy equation have been thoroughly analyzed and reported. From the aforementioned arguments it is explicit that the present work does not follow the conventional approach to report the solutions in terms of constant *Kn* or *Br* or *Pe* (Peclet number), where $Pe = Re.Pr$ indicates the relative dominance of convection over axial conduction. Instead, the analysis focuses on the way rising degree of rarefaction influences the heat transfer phenomena without taking any assumption that does not align with practical conditions. The new insights brought about by this analysis is discussed exhaustively in the sections on results and discussions.

2. Problem definition and the method of analysis

Present study underscores the heat transfer aspects of mildly rarefied slip flows of gaseous Nitrogen through a circular pipe. The primary objective of present work is to observe the dependence of heat transfer phenomena on *Kn*. For this, the analysis is considered particularly with comparable *Kn* throughout the flow domain so that explicit dependence on *Kn* can be given. This is different from the existing literatures where *Kn* and other parameters vary substantially with axial distance but the results are still reported in terms of constant *Kn*. In the present work, the pressure ratio is kept relatively small for all the test cases. Indeed, in a long microchannel, the pressure ratios may range from small to very large values. However, the region influenced by heating either due to the sensor element or due to the other sources would span over a short distance where the *Kn* values would stay comparable. In that short span, the pressure drop would remain small and the presented results would apply well. For the remaining portion of the long microchannel, if subjected to similar heating conditions, the solutions can easily be approached using the approximations of isothermal flow. This has been demonstrated in the results sections 4.1 and 4.4. The schematic of the set-up used for this study with the cylindrical coordinates system is shown in Fig. 1.

In order to ensure the non-imposition of uniform temperature at the inlet to the heating zone, the first half-length of the pipe wall is kept at a temperature of the fluid at the inlet (300 K). This leaves the temperature field at the inlet to the heating zone ($z = 0$) as a part of the solution field

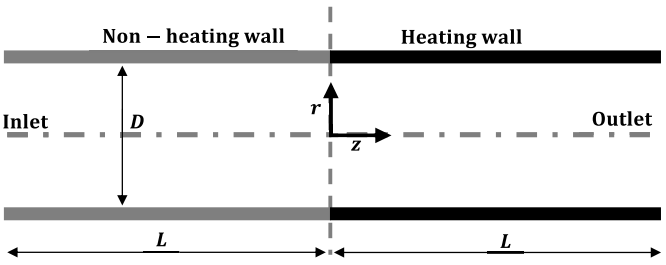

Fig. 1. Schematic of the set-up.

to be determined. This is in accordance with the conventional practice adopted for the heat transfer analysis of the extended Graetz problem [18]. The second half-length of the pipe wall is kept at *350* K. The wall temperature is restricted to *350* K primarily for two reasons: a) The typical heat exchangers at small scale involve comparable temperature ratios as considered in the present work and b) higher temperature ratios would lead to significant variation in all the properties with temperature, which would form a different class of problem. In the study of this problem, several combinations of pipe diameters and lengths have been analyzed while maintaining the same *Kn* and *Re* combination for each test case. The results fall identical in terms of every non-dimensionalized parameter. Hence, the results are reported for one such combination where pipe diameter of D = *1* cm and half-length of L = 0.5 m are used. This high length to diameter ratio affixes the certainty to the locally fully developed hydrodynamic conditions before the flow comes in the region influenced by axial conduction. The governing equations for mass, momentum and total energy used for obtaining the solution field are [19]

$$\frac{\partial \rho}{\partial t} + \nabla \bullet (\rho \boldsymbol{V}) = 0 \tag{1}$$

$$\frac{\partial \rho \boldsymbol{V}}{\partial t} + [\nabla \bullet \rho \boldsymbol{V}\boldsymbol{V}] = -\nabla p - [\nabla \bullet \boldsymbol{\tau}] \tag{2}$$

$$\frac{\partial}{\partial t}\left(\frac{1}{2}\rho v^2 + \rho U\right) + \left(\nabla \bullet \left(\frac{1}{2}\rho v^2 + \rho U\right)\boldsymbol{V}\right) = -(\nabla \bullet \boldsymbol{q}) - (\nabla \bullet p\boldsymbol{V}) - (\nabla \bullet [\boldsymbol{\tau} \bullet \boldsymbol{V}]) \tag{3}$$

Here,

$$\boldsymbol{V} = v_r \boldsymbol{\delta_r} + v_z \boldsymbol{\delta_z} \quad , \nabla = \boldsymbol{\delta_r}\frac{\partial}{\partial r} + \boldsymbol{\delta_z}\frac{\partial}{\partial z} \tag{4}$$

$$\boldsymbol{q} = -k\frac{\partial T}{\partial r}\boldsymbol{\delta_r} - k\frac{\partial T}{\partial z}\boldsymbol{\delta_z} \tag{5}$$

where v_r and v_z are radial and axial velocities respectively, p is pressure, U is specific internal energy, and $\boldsymbol{q}$ is the conduction heat flux. The components of the symmetric viscous stress tensor ($\boldsymbol{\tau}$) for the Newtonian fluids with zero dilatational viscosity are given by

$$\tau_{rr} = -\mu\left[2\frac{\partial v_r}{\partial r}\right] + \frac{2}{3}\mu(\nabla \bullet \boldsymbol{V}), \tau_{\theta\theta} = -\mu\left[2\frac{v_r}{r}\right] + \frac{2}{3}\mu(\nabla \bullet \boldsymbol{V}), \tau_{zz} = -\mu\left[2\frac{\partial v_z}{\partial z}\right] + \frac{2}{3}\mu(\nabla \bullet \boldsymbol{V}), \tau_{rz} = \tau_{zr} = -\mu\left[\frac{\partial v_r}{\partial z} + \frac{\partial v_z}{\partial r}\right] \tag{6}$$

where all the terms with their dependencies in the azimuthal direction have been dropped. In order to incorporate the effects of non-equilibrium at the wall, first order velocity-slip and temperature-jump boundary conditions are used:

$$v_{z,w} = -\frac{2-\sigma_v}{\sigma_v}\lambda\left.\frac{\partial v_z}{\partial r}\right|_w, T_w - T_{f,w} = \frac{2-\sigma_T}{\sigma_T}\frac{2\gamma}{(\gamma+1)}\frac{\lambda}{Pr}\left.\frac{\partial T}{\partial r}\right|_w \tag{7}$$

The values of tangential momentum accommodation coefficient and thermal accommodation coefficient, σ_v and σ_T are each set to *0.9137*. These values fall well within the widely accepted range of values for normal surface conditions [20]. These are also the default values present in the solver.

2.1. The solution method

The governing equations in cylindrical coordinates are solved numerically using the academic version of FLUENT-2020-R2 that uses finite volume formulation of the governing equations over each control volume. Our primary objective is to analyze the slip regime and its extension to the continuum regime. Hence, the analysis is restricted to $Kn < 0.1$. The first order slip and temperature jump boundary conditions present in the solver are suitably useful for flow in the slip regime. The equation of state for gaseous Nitrogen is taken as that of an ideal gas, i.e., $p = \rho RT$. The remaining thermophysical properties in the equations are viscosity (μ), specific heat at constant pressure (c_p), and thermal conductivity (k). The variation of these properties with temperature is supplied in terms of their values at *50* discrete pairs of data points. This database is developed using the NIST based tool REFPROP. The meshing of the flow domain is worked with refinement near the pipe wall, inlet and outlet, and around the inlet to the heating region. For the radial and axial directions, different pairs of grid sizes are tested ranging from $[20 \times 500]$ to $[200 \times 5000]$. Finding that the mesh refinement over $[130 \times 3250]$ does not lead to any observable differences, this combination of mesh sizes is used throughout. SMIPLEC (Semi – Implicit Method for Pressure Linked Equation – Consistent) algorithm is used for each run and the normalized residuals are specified to drop below 10^{-8}. This keeps the sum of linearization and discretization errors near minimum.

Supplied boundary conditions at the inlet and outlet are:

$$\text{At } z = -L: \quad v_z = V_{in}, \; v_r = 0 \text{ ms}^{-1}, \; T = 300 \text{ K} \tag{8}$$

$$\text{At } z = L: \quad p = p_{out}, \; \frac{\partial T}{\partial z} = 0 \text{ Km}^{-1} \tag{9}$$

At the inlet, uniform axial velocity and temperature are specified. Since the inlet is kept sufficiently away from the inlet to the heating region, these specifications do not encounter any limitation in terms of their effect on the phenomena. At the exit, pressure is specified which is used by the algorithm in conjunction with the continuity and momentum equations to yield the complete velocity field. Finally, the last two axial cells are specified the same temperature for each radial location. The specified uniform velocity at the inlet is aimed to keep the pressure ratio less than *1.03* for all the test cases. Assuming an outlet temperature of *350* K and specified pressure boundary condition at the exit, *Kn* at the exit is fixed. This does not, by any means, impose the condition of *350* K at the exit. A uniform temperature of *300* K at the inlet, the equation of state for an ideal gas, the specified passage dimensions (Fig. 1), and the definition of locally fully developed velocity field (Eq. (12)) are used to obtain the mass flow rate and *Re* at the inlet corresponding to each run. This test is then repeated till the desired inlet to outlet pressure ratio is achieved. It ensures comparable *Kn* all along the flow, thus allowing for a generalized discussion of the results in terms of *Kn* and *Re*. This does not hold true for large pressure ratios where the value of *Kn* can change by orders of magnitude from inlet to exit. Table 1 highlights the important parameters (*Kn*, *Re*, *Pe* and *Ma*) present in a few of the important set of test cases studied. Here, *Ma* indicates the ratio of the speed of medium to the speed of sound in the same medium. All these parameters represent the mean values over the complete axial span for each test case. These parameters nearly remain constant over the whole domain except near the inlet to the heating region where they undergo small changes due to changes in the properties with temperature. These changes are small enough that each mean value adequately represents its corresponding test case. For a defined fluid, only two out of these four parameters can be independently prescribed for a particular problem. Thus, it is important to select the pair of independent parameters before presenting the results or making any

Table 1
Important parameters for a few of the test cases.

Kn	*Re*	*Pe*	*Ma*
0.0009	20.51	14.64	0.012423
0.0011	13.15	9.38	0.009956
0.002	4.17	2.98	0.005633
0.003	1.83	1.30	0.003744
0.004	1.03	0.741	0.00283
0.005	0.669	0.478	0.002282
0.006	0.468	0.334	0.001916
0.007	0.347	0.247	0.001655
0.008	0.273	0.195	0.001475
0.009	0.218	0.155	0.001323
0.01	0.173	0.124	0.001185
0.0112	0.142	0.101	0.001076
0.02	0.047	0.033	0.000642
0.03	0.024	0.017	0.000473
0.04	0.014	0.01	0.000378
0.05	0.0095	0.006	0.000324
0.06	0.0072	0.005	0.00029
0.071	0.0053	0.004	0.000257
0.08	0.0045	0.003	0.000242
0.09	0.0037	0.002	0.000227

comparison. As described, the present study selects representative *Kn* and *Re* for each test case, thereby leaving *Ma* and *Pe* as the dependent parameters. Henceforth, any results presented in this work correspond to the representative pairs of *Kn* and *Re* from Table 1. Numerical simulations were conducted for more than *100* cases and the obtained results are discussed in details in section 4 for a few of the representative cases.

3. Validation

It has been described in the last section that the grid convergence tests have been verified. In this section, we present comparison of our results with the experimental results, both for hydrodynamic and thermal fields available in the literature. Experimental determination of average *Nu* with low pressure gas flowing in a tube was first conducted by Demsis et al. [21]. This work was extended by Hemadri et al. [1] where the measurement of centerline temperature variation in the axial direction for the rarefied flows was also carried out. These are among the few reported experimental works on heat transfer associated with mildly rarefied flows. The heating wall temperature used in their case was *339* K and the heating initiated at a distance of *0.08* m from the inlet. All the test cases included in their study have also been studied in the present work. To validate the results from the present work, Fig. 2 (a) shows a comparison of the centerline temperature variation against axial distance with the experimental results from Hemadri et al. [1] for $Kn = 0.00477$. The close agreement between the two results validates our adopted method for the slip regime. The small deviations in the results arise due to the limitations of the Teflon connections placed right on the either side of the experimental set up for thermal insulation. Since preheating of the Teflon wall would take place at the expense of mild cooldown of the heating wall at their junction, there is a slight crossover in the two trends. Due to the preheating of the Teflon wall, the flow should experience larger preheating, thus resulting in upstream shift of the non-isothermal region. All the same, the heating wall near the junction loses some heat, thereby resulting a corresponding drop in temperature below the isothermal wall temperature of *339* K. It should be marked that even before the axial fluid parcels reach the inlet to the heating section, almost *70* % of the temperature difference is already achieved. This suggests that the condition of uniform temperature should not be placed at the inlet to the heating section, particularly when the Mach number (*Ma*) is small ($O \sim (10^{-2})$).

Present work also analyzed few of the cases from the experimental study by Sreekanth [22]. To further validate the approach, Fig. 2 (b) illustrates the comparison of pressure drop for $Kn = 0.011$ and 0.0333. These values correspond to a certain downstream location from the inlet where flow can be treated locally fully developed. Close agreement between the two results for both the cases is explicit. The non-linearity of the pressure-drop owing to compressibility effect and momentum efflux can clearly be observed. For the shown *Kn* cases, neglecting any of these effects leads to severe deviation of the experimental outcomes from the analytical predictions, as well demonstrated by Sreekanth [22]. Since the referred literatures for making comparison and validation are among the few that contain local measurement of quantities, a good match for both the hydrodynamic and thermal quantities ensures sufficient validity of the present work. With our applied method thus validated, we now present some of the interesting findings from this work.

4. Results

Rarefied flows may involve several governing factors that are not present generally in conventional continuum problems. Depending on the type of conditions to which the flow is predisposed, only a combination of these factors play a vital role. The strength of these effects may

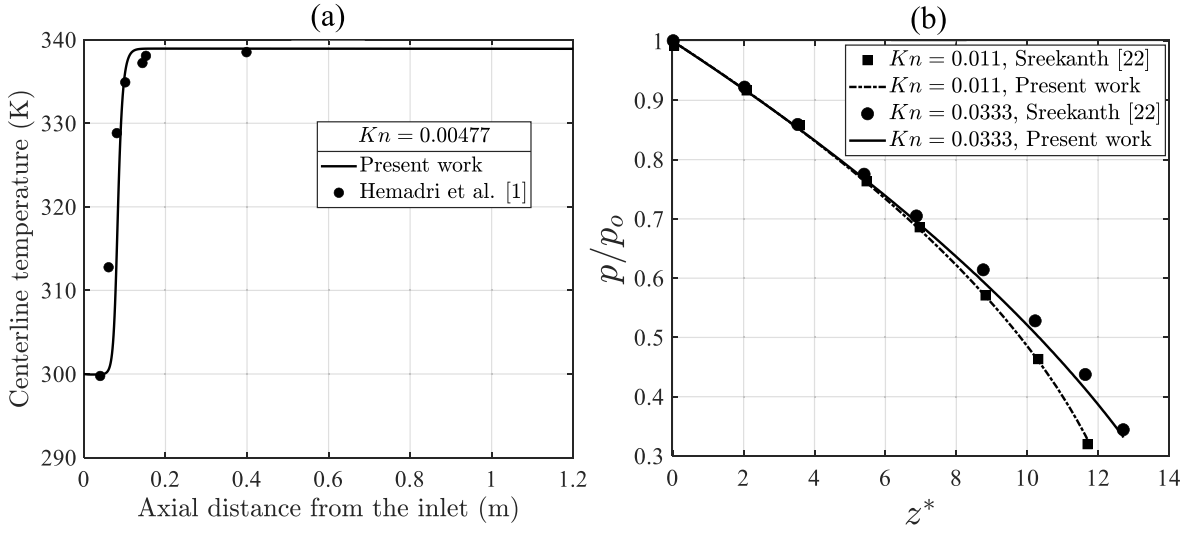

Fig. 2. (a) Comparison of the variation of centerline temperature against axial distance with the experimental results from Hemadri et al. [1] for $Kn = 0.00477$, (b) comparison of pressure drop with experimental results from Sreekanth [22].

itself vary with the location of interest. This section describes the manner in which the flow develops and attains axially unvarying state under the influence of the applied boundary conditions. The development of the thermal field alongside the key defining factors is explained in section 4.1. This is followed by discussions on the influence of viscous stress work at wall and the dependence of *Nu* on *Kn* in section 4.2 and 4.3, respectively. The roles of pressure work and viscous dissipation is described in section 4.4 in context with the flow conditions with relatively lower pressure ratios. Emphasis is laid on the physically inadmissible outcomes that may result due to the assumptions placed before the solution.

4.1. Temperature and velocity fields

The influence of increasing rarefaction on the flow behavior can be well appreciated by visualizing the development of the flow field. This subsection highlights the different regions that develop as the flow progresses alongside the test for the applicability of the conventional locally fully developed velocity field. Comparison of the thermal field along the heating length with rising degree of rarefaction is shown to highlight the dominant effects that define the thermal flow field.

The classical way of testing for the presence of self-similar temperature profiles is to check for the axially non-varying nature of the non-dimensional temperature given by Ref. [23]:

$$\varphi = \frac{T_w - T(r,z)}{T_w - T_{m,z}} \tag{10}$$

The local bulk mean temperature ($T_{m,z}$) is evaluated considering the variation of thermophysical properties in the transverse direction:

$$T_{m,z} = \frac{\int_0^R r\rho(T)v_z(r,z)c_p(T)T(r,z)dr}{\int_0^R r\rho(T)v_z(r,z)c_p(T)dr} \tag{11}$$

Fig. 3 (a) shows the variation of φ with axial distance ($z^* = z/L$) at three different radial locations ($r^* = r/R$) for $Kn = 0.0011$. It can be observed that shortly after the entry to the heating region, the flow indeed achieves a thermally fully developed state where the non-dimensionalized heat transfer coefficients should attain asymptotic values. However, the flow is observed to retain this characteristic for a very short span in the heating region. Thereafter, the flow achieves its second asymptotic state which then prevails till the exit. Similar trends are observed for all the values of *Kn* considered. To represent the case of diminishingly small span of the first fully developed region with increasing *Kn*, the variation of non-dimensionalized axial velocity at the centerline is plotted in Fig. 3 (b) for the highest *Kn* of 0.09.

The sharp rise in the velocity near the inlet to the heating region is explicit. It is due to a corresponding sharp drop in density, brought about by a sharp increase in temperature, as also observed in the experimental result (Fig. 2). If the variation of any of the property is neglected, the magnitudes get largely off from the result shown. For e.g., neglecting the variation of viscosity with temperature yields overprediction due to unaccounted increment in the viscous stresses and neglecting the variation of thermal conductivity shifts this region of influence further downstream. On the either side of this narrow region, the velocity gradient nearly remains constant with a marginally greater value in the latter region. This is due to the increased viscous forces causing higher pressure gradients for the mass flux driven systems. The applicability of the conventional locally fully developed velocity profile in the heating region is also shown in Fig. 3 (b). Its expression is given by Ref. [22]:

$$\frac{v_z}{\bar{v}_z} = \frac{1 + 4C_1Kn - r^2/R^2}{0.5 + 4C_1Kn}, \text{ where } C_1 = \frac{2-\sigma_v}{\sigma_v} \text{ and } \bar{v}_z = \frac{\mu Re}{\rho D} \tag{12}$$

Since the maximum difference in the magnitudes of v_z from the two solutions is obtained at the axis, the comparison is presented for $v_{z,axis}$ along the flow direction. It can be seen that the assumption of locally fully developed velocity profile closely approximates the actual velocity field except in the small region in the vicinity of $z^* = 0$. The small differences between the results develop in the heating region where the transverse variation of density and viscosity are significant. These differences then remain constant throughout the rest of the domain, thus clearly indicating a close prediction by Eq. (12). Hence, the applications where only approximate solutions for v_z are required, Eq. (12) can be used in order to de-couple the momentum balance from the energy balance. To obtain such fields in the narrow range of the heating region, an iterative procedure needs to be carried out between Eq. (12) and the numerical results from the energy equation. However, with further rise in T_w or with rise in *Kn* beyond the slip regime, the differences aggravate and such formulations may fail to work.

The changes in the heat transfer characteristics with increasing *Kn* can well be understood by observing the changes in the temperature field across the whole domain. Towards this, Fig. 4 (a) and (b) present the variation of non-dimensionalized temperature $\left(\theta = \frac{T_w - T}{T_w - T_{in}}\right)$ at the wall and at the axis with axial distance, respectively, for $Kn = 0.002$, 0.006 and 0.09.

Fig. 4 (a) depicts a reduction in the temperature of the fluid at the wall in the heating region as *Kn* increases. This is due to the increasing

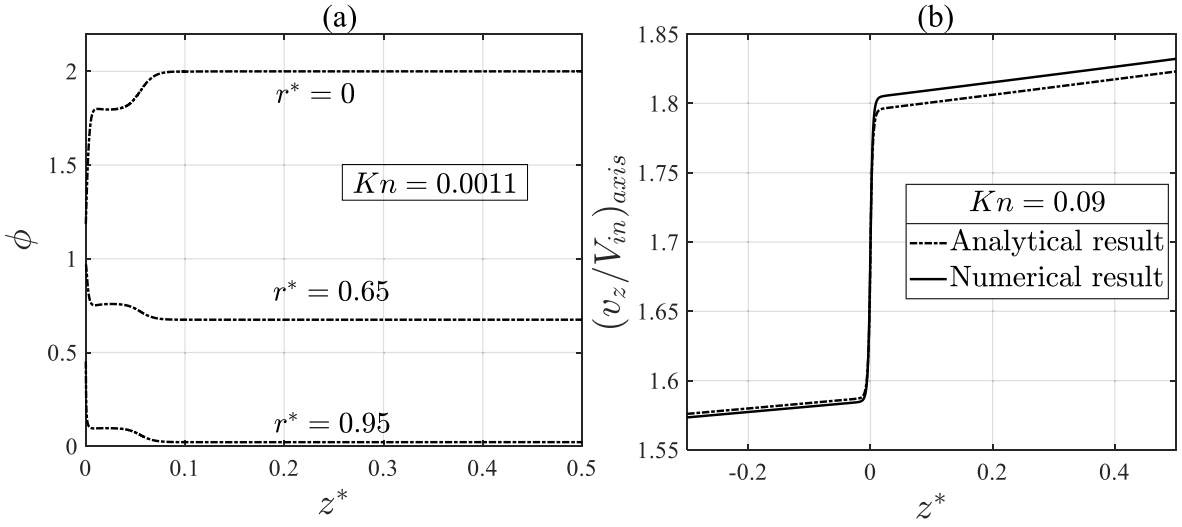

Fig. 3. (a) Variation of non-dimensional temperature φ with axial distance at three different radial locations for $Kn = 0.0011$, (b) variation of non-dimensional axial velocity with axial distance and its comparison with the analytical result from Eq. (12) for $Kn = 0.09$.

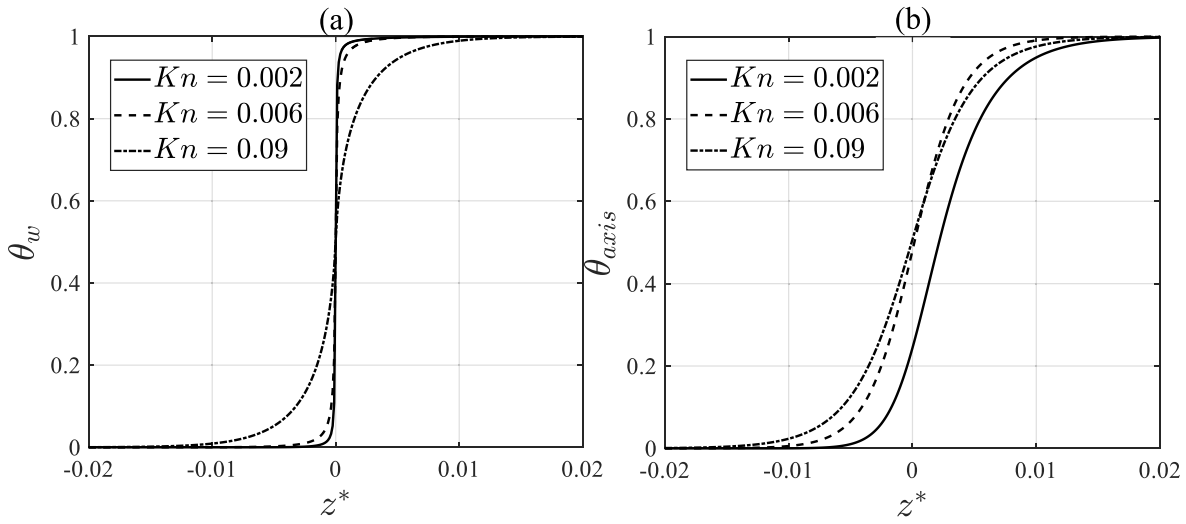

Fig. 4. Variation in fluid temperature with axial distance for $Kn = 0.002, 0.006$ and 0.09 at (a) the wall and (b) the axis.

temperature-jump at the wall. Simultaneously, the fluid parcels in the non-heating region ($z^* < 0$) near the wall are at a greater temperature for higher *Kn* cases owing to enhanced axial conduction in the backward direction. Therefore, the heat transfer from the fluid to the wall in the non-heating region depends on the relative dominance of axial conduction and thermal resistance at the wall due to temperature-jump. In Fig. 4 (b), the temperature pattern at the axis in the non-heating region resembles the behaviour described in Fig. 4 (a). This must be due the dominant axial conduction at the centerline as well, unlike the continuum cases where the axial conduction near the axis is considerably lower than that near the wall due to relatively steep velocity profile [18, 24]. However, the heating region in Fig. 4 (b) does not show any monotonic pattern. At any given axial location little downstream of $z^* = 0$, the rising *Kn* first causes a corresponding rise in the centerline temperature due to enhanced axial conduction. However, any further rise in *Kn* beyond *0.006* causes the temperature-jump at the wall to overcome the heating due to axial conduction, thereby lowering the heat transfer and the temperature.

It comes out that the practice of prescribing a uniform temperature over the cross-section at the inlet to the heating region falls in disagreement with the reality. The specification of thermal boundary condition at the non-heating wall plays vital role in the deciding the temperature near the inlet to the heating region. The primary causes that emerge to influence the flow behavior are axial conduction and temperature-jump at the wall. Thus, any proposal showing monotonically varying strength of heat transfer coefficient with rising *Kn* would yield erroneous calculations both in the heating and the non-heating regions.

4.2. Role of viscous stress work at the wall

Before describing the influence of increasing rarefaction on the heat transfer coefficients, the effects of interaction between the wall and the moving fluid at the wall is briefly discussed in this section. This is an essential factor which decides whether its inclusion in the analysis results to any practically useful outcome or not.

The concept of viscous stress work at the wall was first highlighted by Maslen in 1958 [7] and it was briefly discussed by Sparrow and Lin [4]. In most of the later studies reported, it has been ignored altogether, irrespective of the ranges of *Kn* from inlet to the exit. Hadjiconstantinou included it in the expression for Nu_{fd} for small range of *Br*. Balaj et al. [25] observed that the contribution from the viscous stress work at the wall and the supplied heat flux are comparable both in cooling and heating cases. In the cooling cases, they observed heating of the bulk fluid due to shear work at the wall. In the recent works by Nicolas et al. [16], this term was found to be the cause for temperature gradients to exist near the wall when the convection effect becomes negligible. Assam et al. [26] used the modified temperature jump boundary conditions for the high *Ma* trials that includes this effect. All these studies, however, involved relatively large pressure ratios, thus making the consideration of this effect indispensable. Since the present work emphasizes the conditions with relatively lower pressure ratio, it becomes essential to test for its contribution.

Fig. 5 shows an exaggerated schematic of a small control volume between the pipe wall and the axis with an axial span of *dz*. The actual heat exchange with the wall ($\boldsymbol{q}_{tot}$), the work done by viscous stress force at the wall ($\boldsymbol{q}_{vsw}$), and the total heat diffused inwards ($\boldsymbol{q}_{diff}$) are shown.

Application of net energy balance at the fluid-wall interface reads:

$$\boldsymbol{q}_{tot} + \boldsymbol{q}_{vsw} = \boldsymbol{q}_{diff}, \text{where } \boldsymbol{q}_{diff} = -k\left(\frac{\partial T}{\partial r}\right)_w \boldsymbol{\delta}_r \text{ and } \boldsymbol{q}_{vsw} = (\tau_{rr} v_r + \tau_{rz} v_z)(-\boldsymbol{\delta}_r) \tag{13}$$

For the conditions of stationary wall, the magnitude of $\boldsymbol{q}_{tot}$ can be given as:

$$q_{tot} = k\frac{\partial T}{\partial r}\bigg|_w + \mu v_{z,w}\frac{\partial v_z}{\partial r}\bigg|_w \tag{14}$$

Eq. (14) states that the net heat exchange between the wall and the fluid is different from the inward diffusion of heat where the difference is due to the viscous stress work done at the wall. Based on the radial temperature gradient near the wall, the viscous stress work may either add to inward heat diffusion or it may transfer the generated heat to the

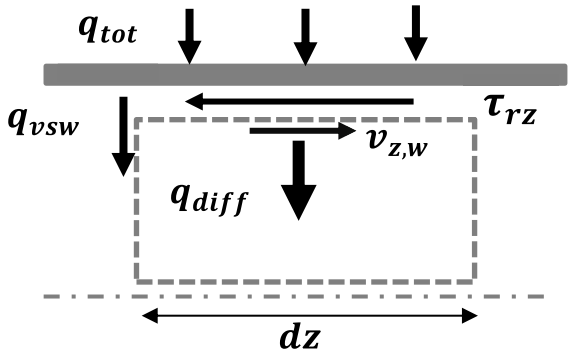

Fig. 5. Schematic of a small control volume of axial span *dz* between the pipe wall and the axis showing energy interaction at the wall.

wall. The expression for Nu to evaluate the non-dimensionalized heat transfer coefficient or temperature gradient at the wall is given by:

$$Nu_{tot} = \frac{q_{tot} D}{k_f (T_w - T_{m,z})} \quad \text{and} \quad Nu_{diff} = \frac{q_{diff} D}{k_f (T_w - T_{m,z})} \tag{15}$$

To demonstrate the strength of viscous stress work for the cases studied in the present work, Fig. 6 (a) represents the variation of local Nu against axial distance for $Kn = 0.0011$ and 0.01. Both Nu_{tot} and Nu_{diff} are shown. In accordance with the nature of the thermal field represented by Fig. 3 (a), Nu follows two distinct asymptotic states shortly after the thermal entrance region in both the cases. The first state indicates the region where the heat flux received from the wall is significant. However, the second state manifests itself with $Nu_{diff} \sim 0$. This indicates almost no inward diffusion of heat received by the fluid. Simultaneously, Nu_{tot} bears its constant negative values from the end of the first asymptotic state onward. This is observed for all the test cases studied. Theoretically, this indicates that the marginally small amount of heat generated due to finite viscous stress work at the wall is transferred to the wall. From the practical standpoint, however, this negligibly small heat transfer represented by Nu_{tot} does not need subtle emphasis. This can be verified from the plot of heat flux due to diffusion and the heat flux due to viscous stress work at the wall in Fig. 6 (b).

As can be examined from the subplot, near the end of the first asymptotic state at an axial distance of $z^* \sim 0.03$, the heat flux in both the forms have attained negligible values. Hence, these effects need not be taken into account in practical scenarios once the flow crosses the first fully developed region. The small negative value of Nu_{tot} manifests due to negligibly small temperature difference $(T_w - T_{m,z})$ in the denominator in Eq. (15). For all the test cases it is observed that the temperature difference drops below 10^{-3} by the end of the first asymptotic state. Fig. 6 (b) also indicates that this location pertains to the condition where q_{diff} starts appearing to be of the order of q_{vsw}, i.e., both $\sim O(0)$. With further increase in Kn, the heat flux diminishes to $\sim O(0)$ values further upstream. The second asymptotic state can be accurately modelled as an isothermal flow which is also confirmed by the discussion on the temperature and velocity distributions plotted in Fig. 3 (a) and (b), respectively.

It can be commented that for the practical situations that do not undergo appreciable pressure drop during the course of heating, the influence of viscous stress work at the wall can conveniently be neglected without any loss of accuracy. Hence, the discussion of the heat transfer characteristics is continued with the definition of $Nu = Nu_{diff}$ hereafter.

4.3. Trends of local and fully developed Nu

With the flow field and viscous stress work thus discussed, the trends of Nu are presented here. The objective is to illuminate the role that the increasing rarefaction and axial conduction play in defining the rate of heat transfer and the span of the fully developed region.

The influence of increasing rarefaction on Nu is shown in Fig. 7 (a) and (b) in the heating and the non-heating regions, respectively. In the heating region, the asymptotic values of Nu and the axial span of this region vary monotonically only on the either side of $Kn \sim 0.006$. Initially, Nu_{fd} increases with an increase in Kn due to the dominance of axial conduction over thermal resistance at the wall. This is also confirmed by the shortening of the axial span of this region in which Nu_{fd} is maintained. Increasing rarefaction beyond this causes the temperature-jump to dominate, thus leading to a reduction in Nu_{fd} and a consequential increase in the extent of this domain.

All the cases can clearly be seen to report zero heat transfer in the second asymptotic state. Similar arguments justify the variation of Nu in the non-heating region. However, in this region, the axial span of the heat transfer occurring from fluid to the wall increases monotonically with rise in Kn. This is essentially due to the unidirectional rise in the relative strength of axial conduction as can be inferred from Pe data in Table 1. The resulting dependence of Nu_{fd} on Kn in the heating region is plotted in Fig. 8 (a). To the best of the authors knowledge, this variation is not reported in any of the existing studies. It must be either due to the assumptions taken towards making the problem solvable or a relatively higher pressure ratio considered or a combination of them.

The plot of Nu_{fd} with Pe is shown in Fig. 8 (b). Starting from the end of the slip regime ($Kn \sim 10^{-1}$), it can be seen that with a decrease in rarefaction, the effect of axial conduction starts becoming important, thus manifesting itself as a rise in Nu_{fd}. This continues till about $Pe \approx 0.33$. However, due to the increasing rate of axial advection with rise in Pe, Nu_{fd} starts dropping beyond this. One demarcating characteristic deserves attention here. Unlike the continuum cases where $Nu_{fd} \approx 4.1$ corresponding to $Pe \approx 1$ [18], in the rarefied flows, $Nu_{fd} \approx 3.96$ corresponds to $Pe \approx 1$. This indicates that even while the axial conduction becomes nearly same as axial advection (*i.e.*, $Pe \approx 1$), the presence of temperature jump leads to a drop in Nu_{fd} for the rarefied flow conditions in comparison with the continuum flow conditions for the same Pe. Also, the maximum Nu_{fd} achieved in slip flow (≈ 4.022) is lower than that in the continuum case, even with $Pe \approx 0.33$. This implies that even with the axial conduction being nearly three times dominant over axial advection, the rarefaction causes Nu_{fd} to drop in comparison

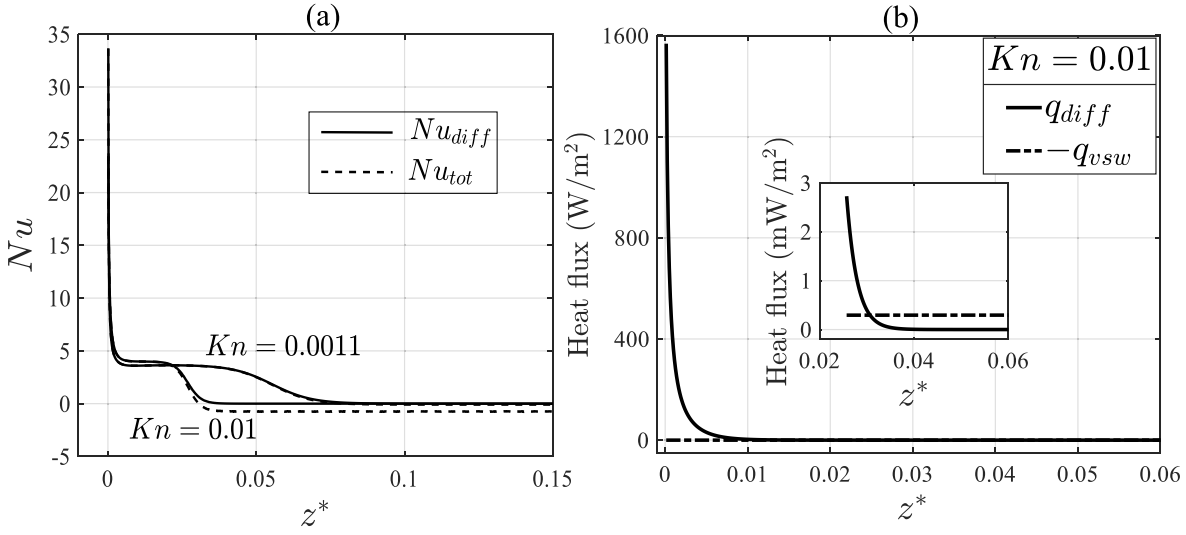

Fig. 6. (a) Nu_{diff} and Nu_{tot} variation for $Kn = 0.0011$ and 0.01, (b) q_{diff} and $-q_{vsw}$ variation for $Kn = 0.01$.

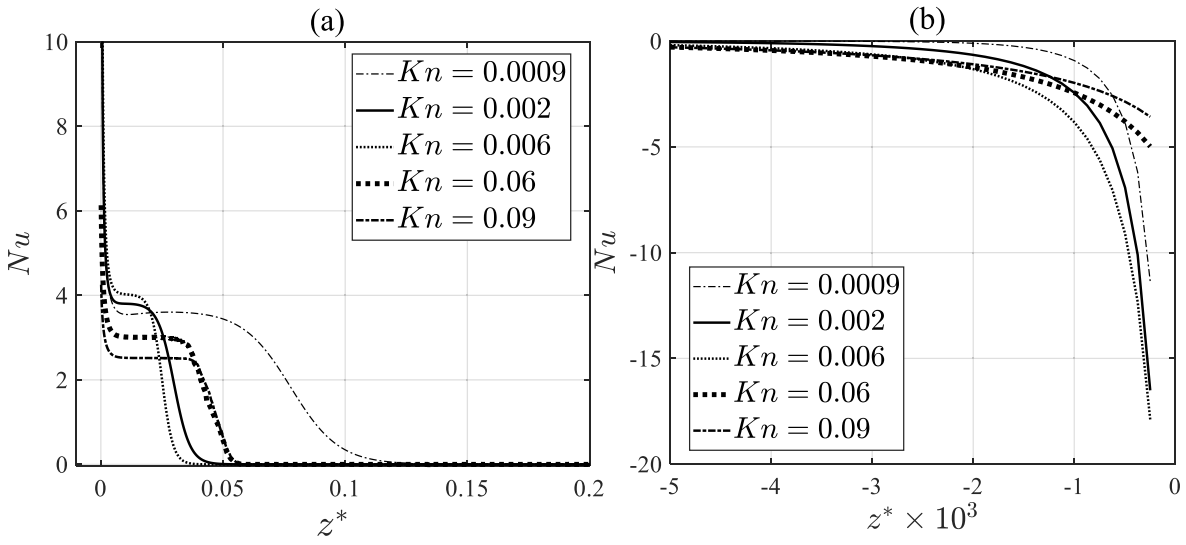

Fig. 7. *Nu* variation for different *Kn* in (a) the heating region and (b) the non-heating region.

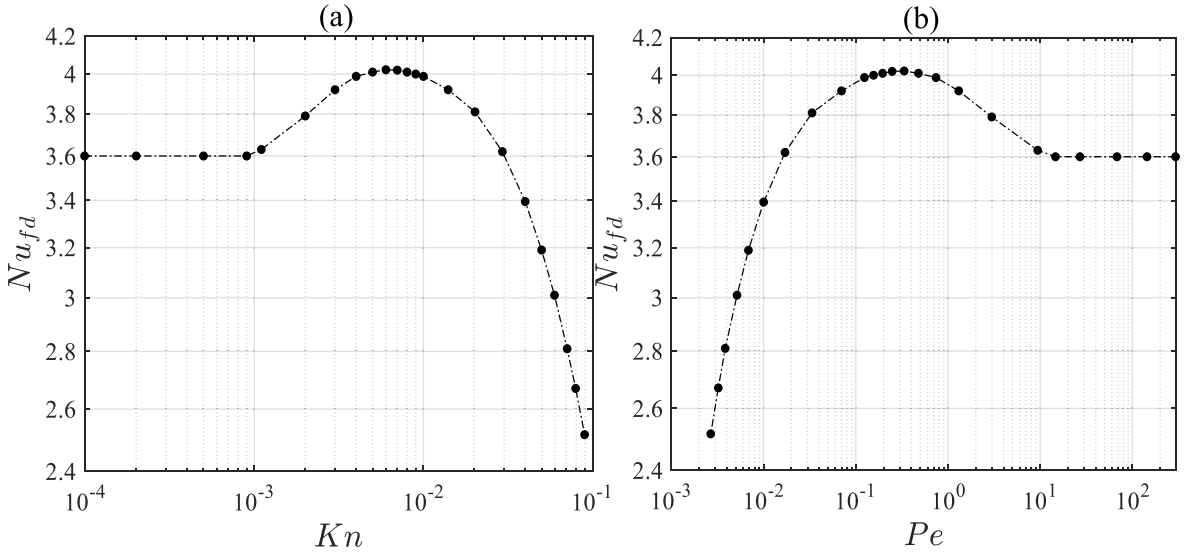

Fig. 8. Variation of Nu_{fd} in the heating region with (a) *Kn* and (b) *Pe*.

with the continuum case. This is an implicit, yet useful observation that should be attended with respect to the influence of rarefaction, i.e., rarefaction always tends to decrease the heat transfer coefficient in comparison with the continuum case for comparable values of similarity parameters.

It should be noted that any presented trends/correlation in the literature which represents a monotonic variation of Nu_{fd} with *Kn* and *Re* may fall erroneous in the applications where the degree of rarefaction remains comparable over the whole domain of interest. The emergence of this heat transfer feature with increasing rarefaction casts useful stress on the practice that should be followed in order to prepare a practical dataset for the dependence of Nu_{fd} on *Kn* and *Re*. It is equally important to shed light on the description of two independent similarity parameters, such as *Kn* and *Re* in the present work. Any variation that shows dependence only on one parameter may fail to expose the complete flow behavior.

4.4. Analysis for the strength of viscous dissipation and pressure work

Since the work reported by Ou and Cheng [5] for the mutually negating effects of pressure work and viscous dissipation, their influence has been rigorously discussed in the literature. However, in many of the available literatures, only one out of these effects has been considered. Even with the literatures discussing these effects together, the underlying assumptions may not describe the flow physics well. This last subsection discusses the role of pressure work and viscous dissipation and about the common mistreatment of these effects with the assumptions that the problem definitions are given.

To quantify the effect of viscous dissipation, *Br* is the conventional similarity parameter. It is defined as the ratio of viscous dissipation to the heat exchange rate with the wall:

$$Br = \frac{\mu \bar{v}_z^2}{k_f \left(T_w - T_{m,z}\right)} \tag{16}$$

Although significantly large number of variations have been reported in the literature for the effect of *Br* on *Nu*, the tests on them being physically admissible depends on the trend that *Br* follows as the flow progresses. In addition, the individual magnitudes of the two effects in Eq. (16) also need to be analyzed before attributing the causes of any of the heat transfer characteristics to the viscous dissipation. To highlight

these aspects, Fig. 9 (a) represents the *Br* profile along the flow for three cases. All the cases represent qualitatively similar patterns where the magnitude of *Br* remains close to zero over major fraction of the heating length. When the received heat flux starts dropping to lower values along the downstream, *Br* shows a corresponding rise. This can be verified from the comparison of *Nu* variation in Fig. 6 (a) and *Br* variation in Fig. 9 (a) for $Kn = 0.0011$. For all the cases it can be observed that the asymptotic value of *Br* approaches unity and is maintained thereafter. Two aspects deserve attention here for the conditions of flow tested in the present work: (a) *Br* never does remain constant along the flow in the heating region and the relations/trends given in the literatures for *Nu* with *Br* may altogether fail to give physically admissible calculations, and (b) the values of $Br \sim 1$ does not indicate that viscous dissipation is defining the temperature field over the flow domain. All the cases report $Br \sim 1$ by the end of the first asymptotic region which is an implication of the negligibly low rate of heat exchange between the wall and the fluid. This can be verified from Fig. 6 (b) with the description presented there. Further, it would be inappropriate to generalize that the increasing rarefaction causes a higher viscous dissipation. Fig. 9 (b) represents radial velocity profiles of v_z at the same axial location $z^* = 0.15$ for $Kn = 0.01, 0.05$, and 0.09. It is explicit that the rising *Kn* tends to flatten the velocity profile, thereby dismissing the needs for rigorous analysis of viscous dissipation for the flows with relatively lower pressure drop.

The quantification of the viscous dissipation terms has been worked out for several test cases in the present work. It is observed that the cases with lower *Kn* ($< 10^{-3}$) and similar pressure drop conditions displays a comparatively strong dependence of the temperature field on viscous dissipation. The consideration of viscous dissipation, albeit, can totally be neglected for the range of *Kn* discussed. These aspects are displayed sufficiently by the radial temperature profiles at discrete axial locations for $Kn = 0.0009$ and 0.09 in Fig. 10 (a) and (b), respectively.

Both the cases support the argument that the temperature variation along the radial direction is negligibly small and its non-consideration in the analysis would not imply any observable offset from the actual field. Even if we consider it for discussion here, the case with higher *Kn* in Fig. 10 (b) shows that the temperature field can be called isothermal when compared to that in Fig. 10 (a). With increasing axial distance, it reports absolutely uniform temperature field. On the contrary, the temperature profile in Fig. 10 (a) shows that the marginally small temperature difference between the axial location and the wall is maintained throughout the rest of the flow. At all the axial locations, the zero temperature gradients present near the wall due to small viscous dissipation confirms no heat exchange whereas the marginally lower temperature near the axis confirms the relative dominance of the expansion work due to pressure drop. Interestingly, there is a small drop in the centerline temperature from $z^* = 0.175$to 0.48 due to expansion work. This corresponds to the first case in Table 1 with the highest $Ma \approx 0.0124$. To analyze the effect of the rate of pressure work for the flow of ideal gases, it becomes inevitable to observe the net rate at which the kinetic energy leaves the control volume by convective transport. This can be addressed by quantifying the terms of the mechanical energy balance for the steady state condition:

$$\left(\nabla \bullet \left(\frac{1}{2}\rho v^2\right)\boldsymbol{V}\right) = -(\boldsymbol{V} \bullet \nabla p) - (\boldsymbol{V} \bullet [\nabla \bullet \boldsymbol{\tau}]) \tag{17}$$

The term on the L.H.S. represents the net rate of outward advection of the kinetic energy (KE_{out}). The first and second terms on the R.H.S. represent the rate of pressure work (*PW*) and viscous stress work (*VSW*) that cause the rate of change in the kinetic energy. The three quantities are plotted in Fig. 11 (a) and (b) for $Kn = 0.0009$ and 0.09 at $z^* = 0.002$. The total rate of work done by the two forces is also plotted to validate the adopted method of analysis.

This comparison shows that pressure work and viscous stress work are negligibly smaller for the higher *Kn* case by about five orders of magnitude. The important aspect to highlight here is the presence of a significant rise in the kinetic energy for lower *Kn* case in comparison with $Kn = 0.09$. As it can be seen, this is due to the dominance of pressure work over the retarding viscous stress work. This expansion work leads to the cooling of ideal gases as well because a rise in the kinetic energy manifests itself as an expansion of the gas. This can be seen from the equation of change for enthalpy. Subtracting Eq. (17) (with the unsteady term added) from Eq. (3), utilizing the relation between enthalpy and internal energy $H = U + p/\rho$ and using the continuity equation (Eq. (1)) gives the equation of change for enthalpy:

$$\frac{\partial \rho H}{\partial t} + (\nabla \bullet (\rho H)\boldsymbol{V}) = -(\nabla \bullet \boldsymbol{q}) - (\boldsymbol{\tau} : \nabla \boldsymbol{V}) + \frac{Dp}{Dt} \tag{18}$$

This equation explicitly states that the pressure work which causes an increase in the kinetic energy also causes a drop in the enthalpy. For ideal gases, a drop in enthalpy implies a drop in temperature but this need not be true for the incompressible flows. It is because this rise in kinetic energy for an incompressible flow merely drops the enthalpy by reducing its 'flow energy' part (p/ρ). This can also be confirmed by using the property relation between enthalpy, pressure and temperature to obtain energy equation in terms of temperature [19]:

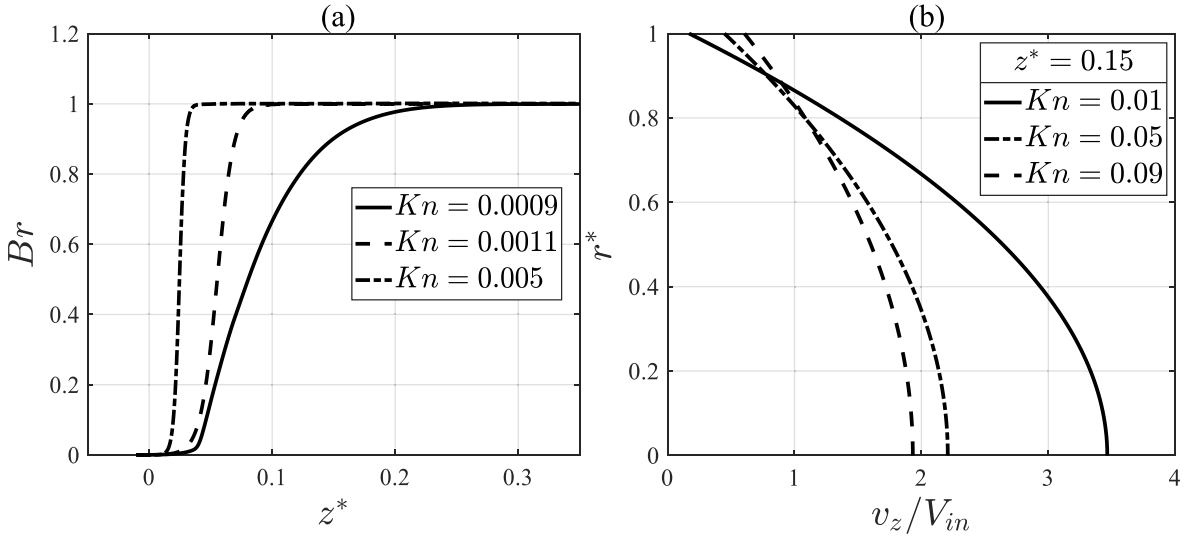

Fig. 9. (a) *Br* profile along the axial distance for $Kn = 0.0009, 0.0011,$ and 0.005, (b) radial velocity profiles for v_z at $z^* = 0.15$ for $Kn = 0.01, 0.05$ and 0.09.

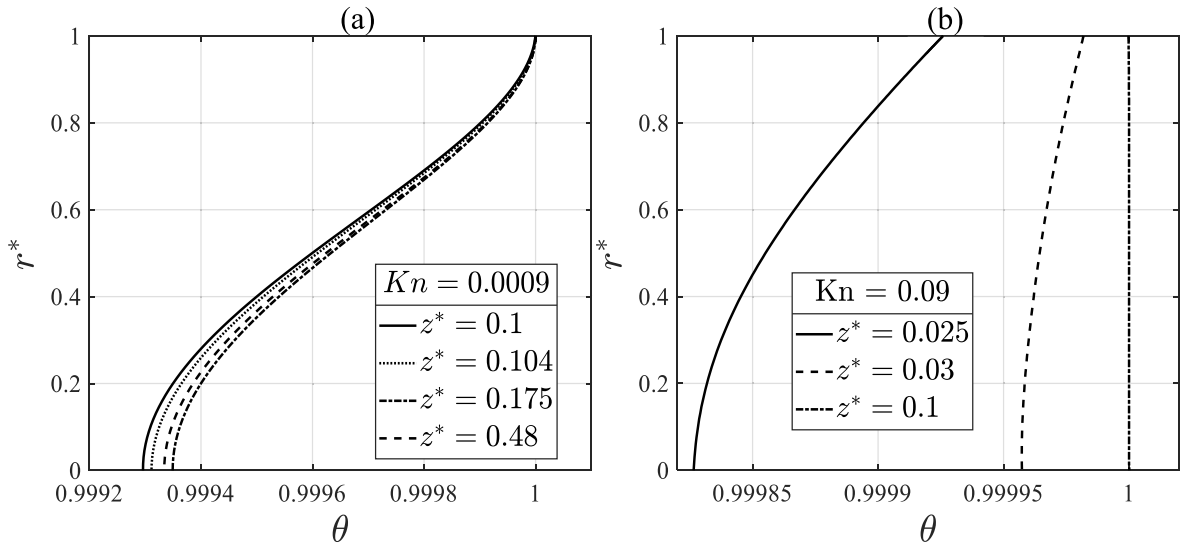

Fig. 10. Radial temperature profiles at different axial locations downstream for (a) $Kn = 0.0009$ and (b) $Kn = 0.09$.

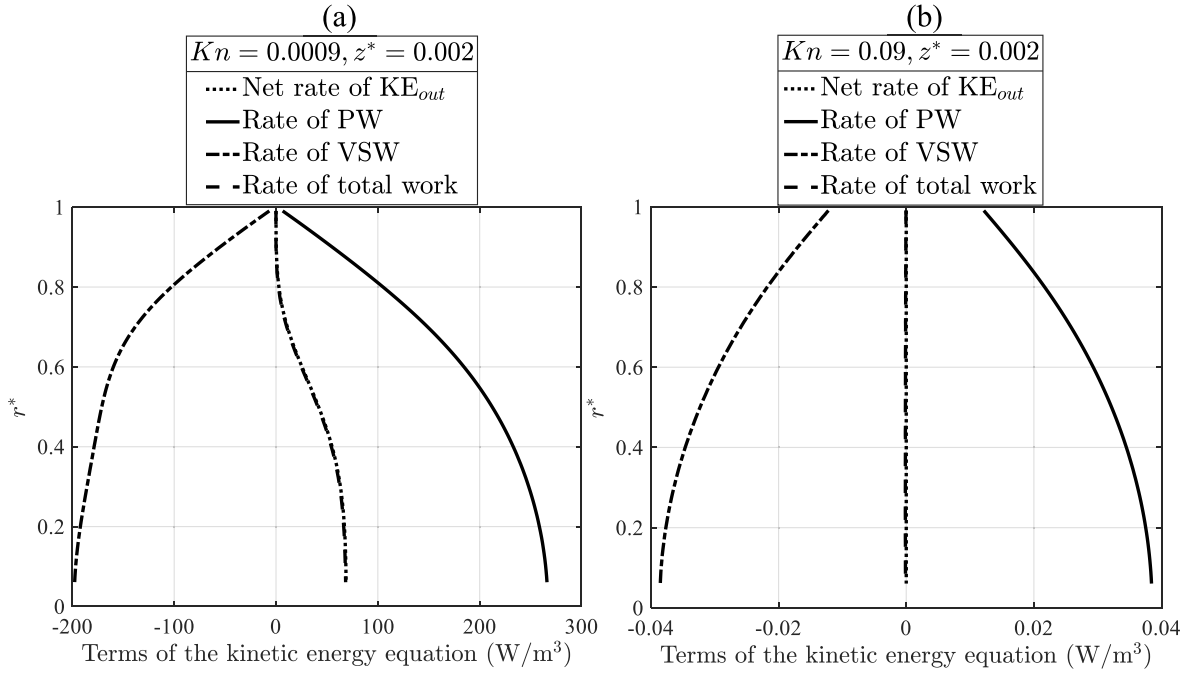

Fig. 11. Terms of the mechanical energy balance vs. radial distance at $z^* = 0.002$ for (a) $Kn = 0.0009$ and (b) $Kn = 0.09$.

$$\rho c_p \frac{DT}{Dt} = -(\nabla \bullet \boldsymbol{q}) - (\boldsymbol{\tau} : \nabla \boldsymbol{V}) - \left(\frac{\partial \ln \rho}{\partial \ln T}\right)_p \frac{Dp}{Dt} \tag{19}$$

It can conclusively be stated that for incompressible flows, the pressure work that causes an increase in the kinetic energy ($\boldsymbol{V} \bullet \nabla p$) will not cause any drop in temperature because $\left(\frac{\partial \ln \rho}{\partial \ln T}\right)_p = -\beta T$ and the coefficient of volume expansion (β) is zero for incompressible fluids. Alternatively, this can be confirmed from equation of change for the internal energy as well where the rate of volumetric dilatation ($\nabla \bullet \boldsymbol{V}$) is zero for an incompressible fluid. Despite this requirement, the rate of pressure work has extensively been reported in most of the available literatures to be the cause of cooling in incompressible flows, while not including the condition of locally fully developed flow. Hence, the assumptions taken to formulate the solution and the relations discussed/derived based on the obtained results may give severely deviated predictions from what is actually present in practical situations.

Referring to Fig. 11 and the description given there, it can be concluded that the rate of pressure work can be neglected for rarefied flows with $Kn > 10^{-3}$ because of negligible increase in the kinetic energy. The small rate at which the velocity rises along the downstream does not add to any net rise in the kinetic energy or the momentum flux. Further, no significant variation in the magnitude of the rate of pressure work and viscous stress work is observed along the radial direction in Fig. 11 (b) in contrast to Fig. 11 (a). This is in agreement with the corresponding temperature profiles observed in Fig. 10. To further illustrate the negligible rate of expansion work for higher Kn cases, the profile of the rate of volumetric dilatation at the centerline is plotted in Fig. 12 for $Kn = 0.0009$ and $Kn = 0.09$.

It is explicit that the fluid parcels experience about two orders higher volumetric dilatation for the lowest Kn case. The rising rate of dilatation before the peak indicates the thermal entrance region where major fraction of the total heat is received.

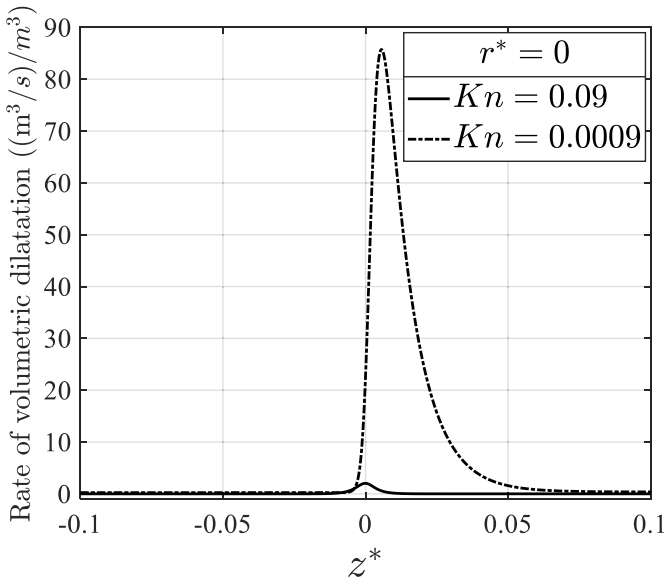

Fig. 12. Profile of the rate of volumetric dilatation for $Kn = 0.0009$ and 0.09 at $r^* = 0$.

The foregoing discussions confirm that the attributes of such flows should not be credited to the pressure work and viscous dissipation effects. The relations reported in the literatures that show the variation of *Nu* with axial distance for fixed values of *Br* do not bring out the true flow behavior; the same flow may experience significantly varying values of *Br* and other parameters. Also, the individual magnitudes of viscous dissipation and heat exchange rates should be reported to comment for their practical importance, instead of stressing only on relative magnitudes of *Br*. Apart from viscous dissipation, the expansion work may be called important in the slip regime only if the pressure ratios are relatively large. As described, this should not be extended to the case of incompressible flows.

5. Discussion

The solutions to the complete governing equations have revealed quite a few interesting findings. The test for self-similarity of the thermal field has shown that the flow attains two asymptotic states after the thermal entrance region. Nearly complete heat transfer takes place by the end of the first asymptotic state. Quantification of the components of the total heat flux helps to visualize that a negligibly small role is played by the viscous stress work at the wall and the heat flux after the first asymptotic state (Fig. 6).

It has been widely observed that the results from the available studies are not in agreement among themselves. Whereas some of the studies reported *Nu* dropping to asymptotic values similar to the continuum cases [4,9,10], others observed two asymptotic states of the flow [11,16], as also observed in the present work. The effect of increasing *Kn* has been reported to reduce Nu_{fd} in all of the available studies, to the best of the authors knowledge. However, the detailed examination in the present work for a large range of *Kn* in the complete slip regime has gleaned the non-monotonous changes in *Nu* with increasing *Kn*. It is found that the thermal flow field and the variation of Nu_{fd} with increasing degree of rarefaction do not show any unidirectional change for the conditions in the present work. Nu_{fd} is found to increase to a maximum value of about 4.022 corresponding to $Kn \approx 0.006$ and $Re \approx 0.468$. This state arises due to the dominance of axial conduction over every other factor. The rising *Nu* with decreasing *Pe* has been elaborately addressed in the available literatures on the extended Graetz problem [18]. Interestingly, for practical purposes, the variation of Nu_{fd} with $Kn \in (0.004 - 0.01)$ and $Re \in (1.03 - 0.173)$can be conveniently ignored in the present problem. Another important understanding is developed by observing the values of Nu_{fd} for same *Pe* values, but corresponding to continuum and rarefied cases. This exposes the monotonic nature of rarefaction in always reducing Nu_{fd} values in the rarefied flow for the same *Pe*. Thus, even with axial conduction being of the same intensity, the role of temperature-jump manifests for the entire slip regime in the form of dropped values of Nu_{fd}. Also, the maximum Nu_{fd} obtained here (4.022) corresponds to $Pe \approx 0.33$ and it is lower than the maximum Nu_{fd} value (4.1) corresponding to $Pe \approx 1$ for the continuum case.

The magnitudes of Nu_{fd} are also not found in agreement in the available studies. Some of the studies report Nu_{fd} values in the range $(4 - 9.6)$ [6,9,10], other studies report relatively lower values in the range $(2 - 4)$ [11,16]. Further, the results in Ref. [16] indicate that Nu_{diff} maintains constant finite value in the range $(2 - 4)$ throughout the second asymptotic state and Nu_{tot} attains nearly zero magnitude in this region. This is in contrast to the findings in Ref. [11] where Nu_{diff} is seen to rise continuously due to increasing rarefaction in the second asymptotic region while maintaining non-zero values. These important differences in the studies primarily arise from the way solution procedures are approached. With the present work, Nu_{diff} is observed to be lower than the values reported in both the studies and approaches nearly zero by the end of the first asymptotic state. Therefore, the conditions of the flow are the key factors that decide the outputs from the designed flow passages and the dependence of *Nu* on *Kn* cannot be generalized. Thus, proper understanding can be developed once the serious and impractical assumptions are lifted, as in the present work.

Apart from the temperature-jump, viscous stress work at the wall and axial conduction, the influence of pressure work and viscous dissipation has extensively been studied in the past. The trends of *Nu* with *Br* for constant *Pe* and similar other cases exist amply. However, such dependencies are subjected to serious limitations with regard to their use inasmuch as none of these parameters independently stay constant as the flow progresses. Neither a rise in rarefaction amounts to growing viscous dissipation, nor a higher *Br* indicates this. These details are sufficiently explained in the description behind Figs. 9 and 10. For the pressure work to decrease the enthalpy, the net rise in the kinetic energy manifests itself as a suitable tool for validation. Its comparison between the low and high *Kn* cases reveals that the expansion work too can be ignored for the slip regime, provided that *Kn* remains comparable over the domain of interest. This can also be confirmed from the quasi-linear rise in v_z in the second asymptotic region of Fig. 3 (b). Many of the literatures have prescribed the serious limitation of incompressible slip flow. At the same time, the influence of expansion work has been observed to be among the primary defining factors for their outcomes. This lies in strict contradiction with the physical requirement where no change in the internal energy should result due to the pressure-drop for an incompressible fluid.

Therefore, immense care needs to be laid on the development of the miniaturized devices involving heat transfer. The operating conditions to which the flow may get exposed should be analyzed thoroughly. This should be followed by a detailed examination of the influence of different terms in the governing equations. The cases with comparable *Kn* along the complete flow domain have been reported in the present work. It is encouraged to rigorously examine the conditions with substantial variations in *Kn* to yield unanimously agreeing outcomes. The outputs should always be reported in terms of two independent similarity parameters, as done in the present work in terms of *Kn* and *Re*.

6. Conclusions

In this work, the heat transfer characteristics of mildly rarefied gaseous Nitrogen flow through an isothermally heated circular pipe is analyzed. Unlike the regular practice of imposing uniform temperature boundary condition at the inlet to the heating region, the problem is studied by dividing the conditions at the pipe wall into two halves. The

first half is maintained at a temperature at which fluid enters the system (300 K) and the second half is maintained at a heating wall temperature of 350 K. Complete form of the governing equations for mass, momentum and total energy in the cylindrical coordinates system are solved. The variation of thermophysical properties with temperature is retained in the analysis. The results are validated by comparing the results of centerline temperature profile with that from the first experimental measurements made by Hemadri et al. [1] for $Kn = 0.00477$.

Following are the primary outcomes that emerge:

- From the test for the self-similarity of the thermal field it is found that after the thermal entrance region, the flow attains two asymptotic states.
- The nature of the temperature field with increasing rarefaction is observed to be dependent on the relative dominance of thermal resistance at the wall and the axial conduction. For rising Kn till about 0.006, the centerline temperature in the heating region is observed to increase whereas any further rarefaction causes it to drop. For the non-heating region, the rising Kn always leads to an increase in the backward penetration of heat and higher temperature at any given axial location.
- Both the heating and the non-heating regions experience maxima in the magnitude of Nu with increasing rarefaction before starting to drop monotonically. The axial span of the first asymptotic state also follows this in the heating region. This is, however not followed in the non-heating region.
- For same value of Pe in the continuum and rarefied regime, Nu_{fd} is found to be lower in the rarefied cases. The maxima in $Nu_{fd} \approx 4.022$ is obtained at much lower $Pe\ (\approx 0.33)$ for rarefied flow cases, even while being smaller than $Nu_{fd} \approx 4.1$ for the continuum flows corresponding to $Pe \approx 1$.
- The strength of viscous stress work at the wall is found to be negligibly small for practical consideration. It has been verified that a rise in Br does not represent strong viscous dissipation and its contribution does not carry any observable role in defining the temperature field.
- The rate of increase in the kinetic energy due to convective transport is found to be negligibly small for higher Kn cases. This has also been verified from the profile for the rate of volumetric dilatation at the centerline. It is found to be smaller by about two orders of magnitudes for $Kn = 0.09$ than $Kn = 0.0009$. Thus, the rate of pressure work can also be ignored for such cases.

Conclusively, it can be hypothesized that for designing the passages for small scale heat exchangers or for the rarefied flow of ideal gases where Kn remains comparable over the domain of interest, attention should be laid carefully on the effects of thermal resistance at the wall and the axial conduction. For these scenarios, the effects of viscous stress work at the wall, rate of pressure work and viscous dissipation can be neglected without any loss of accuracy. Further, a thorough analysis should be exercised before imposing the assumptions on the problem to obtain its solution. This would ensure no subtle faults in the solutions that may altogether neglect the important outcomes which are otherwise present. The cases where pressure drop is considerable forms a different class of problem and the relations given for Nu with Br and Kn should thoroughly be tested for various conditions imposed on the flow.

Declaration of competing interest

The authors declare that they have no known competing financial interests or personal relationships that could have appeared to influence the work reported in this paper.

Data availability

Data will be made available on request.

References

[1] V. Hemadri, G.S. Biradar, N. Shah, R. Garg, U.V. Bhandarkar, A. Agrawal, Experimental study of heat transfer in rarefied gas flow in a circular tube with constant wall temperature, Exp. Therm. Fluid Sci. 93 (2018) 326–333.

[2] A. Agrawal, H.M. Kushwaha, R.S. Jadhav, *Microscale Flow and Heat Transfer*. Mechanical Engineering Series, Springer, 2020.

[3] S.G. Kandlikar, S. Garimella, D. Li, S. Colin, M. King, Heat Transfer and Fluid Flow in Minichannels and Microchannels, 2014.

[4] E.M. Sparrow, S.H. Lin, Laminar heat transfer in tubes under slip-flow conditions, J. Heat Tran. 84 (4) (1962) 363–369.

[5] J.W. Ou, K.C. Cheng, Effects of pressure work and viscous dissipation on Graetz problem for gas flows in parallel-plate channels, Wärme - und Stoffübertragung 6 (4) (1973) 191–198, https://doi.org/10.1007/BF02575264.

[6] N.G. Hadjiconstantinou, Dissipation in small scale gaseous flows, J. Heat Tran. 125 (5) (2003) 944–947.

[7] S.H. Maslen, On heat transfer in slip flow, J. Aeronaut. Sci. 25 (1958) 400–401.

[8] C. Hong, Y. Asako, Some considerations on thermal boundary condition of slip flow, Int. J. Heat Mass Tran. 53 (15–16) (2010) 3075–3079.

[9] H.E. Jeong, J.T. Jeong, Extended Graetz problem including axial conduction and viscous dissipation in microtube, J. Mech. Sci. Technol. 20 (1) (2006) 158–166.

[10] B. Cetin, A.G. Yazicioglu, S. Kakac, Fluid flow in microtubes with axial conduction including rarefaction and viscous dissipation, Int. Commun. Heat Mass Tran. 35 (5) (2008) 535–544.

[11] Z. Sun, Y. Jaluria, Convective heat transfer in pressure-driven nitrogen slip flows in long microchannels: the effects of pressure work and viscous dissipation, Int. J. Heat Mass Tran. 55 (13–14) (2012) 3488–3497.

[12] M. Turkyilmazoglu, Slip flow and heat transfer over a specific wedge: an exactly solvable Falkner–Skan equation, J. Eng. Math. 92 (1) (2015) 73–81.

[13] M. Turkyilmazoglu, Exact multiple solutions for the slip flow and heat transfer in a converging channel, J. Heat Tran. 137 (10) (2015) 1–8.

[14] Y. Haddout, J. Lahjomri, The extended Graetz problem for a gaseous slip flow in micropipe and parallel-plate microchannel with heating section of finite length: effects of axial conduction, viscous dissipation and pressure work, Int. J. Heat Mass Tran. 80 (2015) 673–687.

[15] K.M. Ramadan, Effects of pressure work, viscous dissipation, shear work and axial conduction on convective heat transfer in a microtube, Case Stud. Therm. Eng. 10 (2017) 370–381. July.

[16] X. Nicolas, E. Chénier, C. Tchekiken, G. Lauriat, Revisited analysis of gas convection and heat transfer in micro channels: influence of viscous stress power at wall on Nusselt number, Int. J. Therm. Sci. 134 (May) (2018) 565–584.

[17] I. Guranov, S. Milićev, N. Stevanović, Non-isothermal rarefied gas flow in microtube with constant wall temperature, Adv. Mech. Eng. 13 (11) (2021) 1–9.

[18] A.A. Jha, A. Agrawal, Hydrodynamic and heat transfer aspects of low Peclet gaseous flows through an isothermally heated pipe, AIP Adv. 12 (4) (2022), 045113.

[19] R.B. Bird, W.E. Stewart, E.N. Lightfoot, Transport Phenomena, second ed., J. Wiley and Sons, Hoboken., 2002.

[20] A. Agrawal, S.V. Prabhu, Survey on measurement of tangential momentum accommodation coefficient, J. Vac. Sci. Technol. 26 (4) (2008) 634–645. A Vacuum, Surfaces, Film.

[21] A. Demsis, B. Verma, S.V. Prabhu, A. Agrawal, Experimental determination of heat transfer coefficient in the slip regime and its anomalously low value, Phys. Rev. E - Stat. Nonlinear Soft Matter Phys. 80 (1) (2009) 1–8.

[22] A.K. Sreekanth, Slip flow through long circular tubes, in: Proceedings of the Sixth International Symposium on Rarefied Gas Dynamics, 1969, pp. 667–680.

[23] W.M. Kays, M.E. Crawford, Convective Heat and Mass Transfer, third ed., McGraw-Hill, 1993.

[24] M. Turkyilmazoglu, Heat transport in shear-driven flow with axial conduction, J. Taiwan Inst. Chem. Eng. 123 (2021) 96–103, https://doi.org/10.1016/j.jtice.2021.05.038 [Online]. Available:.

[25] M. Balaj, E. Roohi, H. Akhlaghi, Effects of shear work on non-equilibrium heat transfer characteristics of rarefied gas flows through micro/nanochannels, Int. J. Heat Mass Tran. 83 (2015) 69–74.

[26] A. Assam, N. Kalkote, N. Dongari, V. Eswaran, Investigation of non-equilibrium boundary conditions considering sliding friction for micro/nano flows, Int. J. Numer. Methods Heat Fluid Flow 29 (8) (2019) 2501–2523.

Nomenclature

Br: Brinkman number $\equiv \mu\bar{v}_z^2/k_f(T_w - T_{m,z})$
c: Specific heat (J/kgK), speed of sound (m/s)
D: Diameter (m)
H: Specific enthalpy (J/kg)
k: Thermal conductivity (W/mK)
Kn: Knudsen number $\equiv \lambda/D$
L: Half-length of the pipe (m)
Ma: Mach number $\equiv v_z/c$
Nu: Nusselt number $\equiv D(\partial T/\partial r)_w/(T_w - T_{m,z})$
p: Pressure (Pa)
Pe: Peclet number $\equiv Re.Pr$
Pr: Prandtl number $\equiv \mu c_p/k_f$
q: Heat flux (W/m^2)
R: Radius (m)
Re: Reynolds number $\equiv \rho\bar{v}_z D/\mu$
T: Temperature (K)
U: Specific internal energy (J/kg)
v: Velocity (m/s)
$\bar{v}$: Mean velocity (m/s)

Subscripts

avg: Average of inlet and outlet
diff: Due to diffusion
f: For fluid
fd: Fully developed
in: At the inlet
m: Bulk mean at a cross-section
out: At the outlet
p: At constant pressure
r: In the radial direction
tot: Net exchange from the wall
vsw: Viscous stress work
w: At the wall
z: In the axial direction

Greek letters

β: Coefficient of volume expansion (K^{-1})
δ: Unit vector
λ: Ratio of specific heat at constant pressure and constant volume, mean free path (m)
μ: Viscosity (Pa.s)
ν: Specific volume (m^3/kg)
φ: Non-dimensionalized temperature$\equiv (T_w - T)/(T_w - T_{m,z})$
σ_T: Thermal accommodation coefficient
σ_v: Tangential momentum accommodation coefficient
τ: Viscous stress tensor (Pa.s)
θ: Non-dimensionalized temperature$\equiv (T_w - T)/(T_w - T_{in})$